Translocation of Soft Phytoglycogen Nanoparticles through Solid-State Nanochannels

Journal:	*Journal of Materials Chemistry B*
Manuscript ID	TB-ART-05-2019-001048.R2
Article Type:	Paper
Date Submitted by the Author:	12-Aug-2019
Complete List of Authors:	Lenart, William; Case Western Reserve University, Macromolecular Science and Engineering Kong, Weiwei; Case Western Reserve University, Macromolecular Science and Engineering Oltjen, William; Case Western Reserve University, Macromolecular Science and Engineering Hore, Michael; Case Western Reserve University, Macromolecular Science and Engineering

SCHOLARONE™
Manuscripts

Journal Name

Translocation of Soft Phytoglycogen Nanoparticles through Solid-State Nanochannels

William R. Lenart,[a] Weiwei Kong,[a] William C. Oltjen,[a] and Michael J. A. Hore[a,*]

Phytoglycogen nanoparticles are soft, naturally-derived nanomaterials with a highly uniform size near 35 nm. Their interior is composed of a highly-branched polysaccharide core that contains more than 200 % of its dry mass in water. In this work, we measure the translocation of phytoglycogen particles by observing blockade events they create when occluding solid-state nanochannels with diameters between 60 and 100 nm. The translocation signals are interpreted using Poisson-Nernst-Planck calculations with a "hardness parameter" that describes the extent to which solvent can penetrate through the interior of the particles. Theory and experiment were found to be in *quantitative* agreement, allowing us to extract physical characteristics of the particles on a per particle basis.

1 Introduction

Translocation – the movement of material through narrow regions – is ubiquitous in nature.[1] In cells, translocation is a key process in transporting material from the cellular matrix through the nuclear pore complex into the nucleus. In plant cells, specifically, small channels in the cell wall referred to as plasmodesmata provide pathways for the transport of nutrients throughout the organism.[2] Unfortunately, the plasmodesmata are also pathways for viral infection of plants.[3] In other systems, proteins can self-assemble into channels that facilitate viral infection. For example, the rice dwarf virus, which has a diameter of about 75 nm, moves through Pns10 protein channels with diameters of 85 nm as it infects neighbouring cells.[4] What is noteworthy in this example is the similar length scales between the size of the virus, and the size of the channel. Outside of biological systems, translocation is also a fundamental aspect of water filtration. Given these examples, it is clear that there is a critical need for understanding the translocation of polymers and particles through confining nanochannels, whether for food source security, water purification, or sensing applications.

Translocation measurements of polymers were first reported over 20 years ago.[5] In recent years, translocation, or "resistive pulse sensing", has been suggested as a means to measure physical properties of polymers and nanoparticles. For example, translocation has been suggested as a method for sequencing complex molecules, including DNA and block polymers.[6–8] Venta *et al.*[9] studied the translocation of Au nanorods to deter-

mine their surface charge, and Goyal *et al.* studied single, Au nanosphere diffusion via translocation.[10] For soft nanoparticles, such as liposomes, translocation measurements have been able to detect deformation of the particles in the presence of an electric field.[11] Translocation measurements are typically performed using Coulter counter-type instrumentation, where ionic current through one or more pores/channels is monitored as a function of time. When a particle enters the channel, it blocks the movement of ions through the channel, and a "resistive pulse" is observed that is characterized by a sharp drop in the ionic current. The amplitude of the pulse ("blockade current", Δi) can be related to the size of the particle relative to the channel diameter, and the duration of the pulse ("dwell time", τ) is related to the mobility of the particle. Unfortunately, interpreting a resistive pulse to obtain chemical, structural, or other information is often a challenging task.

Despite the wealth of translocation studies throughout the literature,[1] relatively few studies have investigated nanoparticle translocation, especially for the case of soft nanoparticles. Phytoglycogen particles are low polydispersity polysaccharide nanoparticles ($d_{NP} \approx 35$ nm) composed of highly branched glucose units and isolated from sweet corn kernels. They have been suggested as attractive candidates for use in the cosmetic industry, among others. Recent work from Nickels *et al.*[12] investigated the structural characteristics of phytoglycogen nanoparticles using a combination of small-angle neutron scattering (SANS) and quasielastic neutron scattering (QENS). SANS measurements found that the particles had uniform density, and by varying the scattering contrast in the system, the authors of this study concluded that phytoglycogen nanoparticles are highly hydrated and contain more than 250% of their mass in water. The authors used QENS

a Department of Macromolecular Science and Engineering, Case Western Reserve University, Cleveland, OH, USA.

∗ Corresponding author. E-mail: hore@case.edu

measurements to study the dynamics of water in the nanoparticles, and found that the hydrated water exhibited substantially slower dynamics than free water. Another study of the rheological properties of phytoglycogen particles found that although SANS showed them to be spheres with uniform density, their compression modulus ($K_p \approx 15$ kPa) and behavior under flow suggest that they share many similarities with star polymers and hairy colloids.[13] Other work has investigated the behavior of phytoglycogen as it is swelled with water.[14]

Given that phytoglycogen particles interact strongly with water, and have characteristics in common with both spherical colloids and star polymers, we hypothesized that translocation measurements could yield additional information regarding the internal structure of the nanoparticles. In this work, we perform translocation measurements on phytoglycogen nanoparticles through 100 nm long solid-state Si_3N_4 nanochannels, and interpret the translocation signals by way of calculations using the Poisson-Nernst-Planck (PNP) formalism. The phytoglycogen translocation characteristics are compared to a SiO_2 nanoparticle standard, which is also used to experimentally validate the PNP predictions. Our PNP calculations are in excellent *quantitative* agreement with experimental values, and allow us to determine the percentage of each particle that is water on an individual particle basis. Our results confirm the uniformity of phytoglycogen nanoparticles, and also demonstrate the application of translocation measurement for determining physical properties of soft nanoparticles.

2 Experimental Methods

Phytoglycogen nanoparticles (physical diameter $d_{NP} = 35$ nm, hydrodynamic diameter $D_h \approx 62$ nm) were donated by Mirexus, Inc. (Guelph, Canada). HPLC grade water (Fisher Scientific) was used for all measurements, and passed through a 0.2 μm filter prior to use. 1 M KCl solutions were prepared in a volumetric flask using VWR ACS Grade KCl. Ludox AM-30 SiO_2 nanoparticles were obtained from Sigma Aldrich as a 30 wt% solution in water.

The translocation solution cell is made from poly(tetrafluoroethylene) (PTFE) and consists of two halves each containing a circular well with a channel to connect to the other half. One side contains a small inset in the outer wall around the channel to accommodate the fluoroelastomer gasket used to form the seal around the membrane containing the nanochannel. The membranes (4×5 mm^2) were manufactured by Goeppert, Inc. and consist of a 100 nm thick Si_3N_4 layer (the length of the nanochannel) deposited on 250 μm of fused SiO_2 with a 65 μm diameter window. The channels were etched with a focused electron beam in a transmission electron microscope (TEM). TEM images of the final nanochannels are shown in Figure 1, with intensity histograms in the inset confirming the nanochannel diameters. Ag/AgCl electrodes were prepared by passing electrical current through a 0.5 mm diameter Ag wire in a 1 M KCl solution (Alfa Aesar annealed, 99.9% metals basis). The total length of silver wire for the reference electrode was 82.5 mm, with 51 mm wrapped around the gold lead and 9.5 mm coated in AgCl. The headstage had the same dimensions for the wrapping and AgCl but the overall length was 102 mm. The AgCl portion of the electrodes was coated with a small layer of
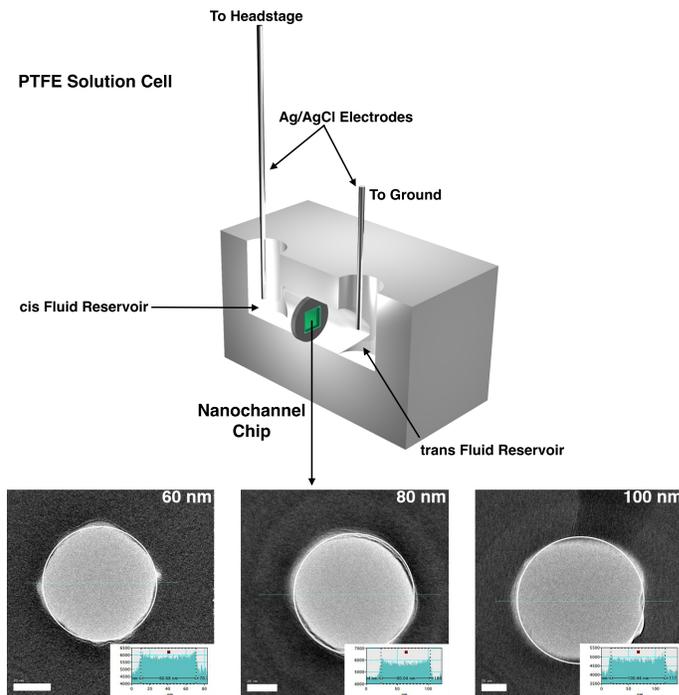
Fig. 1 Cross-sectional schematic of the poly(tetrafluoroethylene) (PTFE) solution cell used for translocation measurements. Nanoparticles are loaded into the *cis* fluid reservoir, and translocate through a nanochannel into the *trans* fluid reservoir. The bottom transmission electron micrographs show the three nanochannels used in this work. In the insets, intensity histograms confirm the nanochannel diameters. Scale bars are 20 nm.

3% w/w agarose(Fisher Molecular Biology Grade Agarose) to reduce fouling of the electrode. A schematic of the experimental apparatus is shown in Figure 1. In this configuration, chloride ions flow towards the headstage electrode, and potassium ions flow towards the grounded electrode. The channel is not ion selective.

All phytoglycogen translocation measurements were performed in a 1 M KCl solution, which is sufficient to screen any charges on the nanoparticle surface. At this salt concentration, the Debye length in the system is $\kappa^{-1} = 0.43$ nm. Although it has been observed that electroosmotic effects can be present in channels larger than the Debye length,[9,15] because of the small Debye length, and large nanochannel diameters relative to the particle size, we expect that the effects of electro-osmotic flow of ions are negligible. Phase analysis light scattering measurements (Möbiuζ, Wyatt Technology Corporation) could not determine an electrophoretic mobility for the nanoparticles in the presence of 1 M KCl. Thus, we expect motion of the particles to be purely Brownian. SiO_2 samples were prepared in a 1 M KCl, 1 M EDTA dipotassium salt (VWR Ultra Pure EDTA dipotassium salt) solution adjusted to a pH of 14 with the addition of the appropriate amount of 5 M KOH (Dot Scientific Potassium Hydroxide). A pH of 14 was necessary to stabilize the particles in the salt solution. Measurements were taken using an Axopatch 200B patch-clamp amplifier and a Digidata 1550B data acquisition system (Molecular Devices, Inc.) with a 0.1 V voltage bias applied across the

solution cell. Data were obtained in the whole cell configuration ($\beta = 1$) at a sampling rate of 100 kHz with a $10\times$ output gain. A 10 kHz lowpass Bessel filter was applied. Data were collected using the Axoscope 10.6 software package. During measurements, the headstage was placed on a Pb dampening brick to minimize vibrations contributing to signal noise. A wire-wrapping tool was used to securely connect the clean end of the silver wire to the gold electrode lead of the headstage and reference electrodes. The entire experimental apparatus was placed on a vibration isolation table, and enclosed in a Faraday cage. Translocation measurements were post-processed using the OpenNanopore software package.[16]

3 Theoretical Methods

To calculate the magnitude of the ionic current blockage, we utilized the Poisson-Nernst-Planck (PNP) formalism[17,18] using a GPU-accelerated, in-house code. The program is run on NVIDIA Tesla P100 and V100 GPUs. To simulate translocation events, we create a single nanochannel with a tunable diameter d_p and a fixed length of $l_p = 100$ nm. The PNP equations are solved for a simulation box that is $L_x \times L_y = 2000 \times 2000 \ \mu m^2$, and which is collocated on a 512×512 mesh. The choice of mesh size limits our spatial resolution to approximately 4 nm. The lateral size of the simulation box is chosen to be at least $10\times$ the diameter of the nanochannel. A single nanoparticle is placed along the axis of the nanochannel, and the ionic current through the channel is calculated as a function of nanoparticle position. Within PNP, the electrostatic potential (φ) is first calculated from the Poisson equation:

$$\nabla \cdot [\varepsilon(\mathbf{r})\nabla\varphi(\mathbf{r})] = -\frac{\rho_m(\mathbf{r})}{\varepsilon_0} \tag{1}$$

where $\rho_m(\mathbf{r})$ is the total mobile charge carrier density, $\varepsilon(\mathbf{r})$ the relative permittivity in the system, and ε_0 is the permittivity of free space. We set $\varepsilon(\mathbf{r}) = 2$ for the walls of the nanochannel, and $\varepsilon(\mathbf{r}) = 80$ for regions that contain solvent. To model the phytoglycogen nanoparticles, which contain both polymer and water, we set $\varepsilon(\mathbf{r}) = h_{NP} \times 2 + (1 - h_{NP}) \times 80$, where h_{NP} is a "hardness parameter" between 0 and 1 that defines how much the solvent can penetrate the nanoparticle. For example, a solid SiO_2 nanoparticle has $h_{NP} = 1$ while a nanoparticle which blocks 15% of the ion flux has $h_{NP} = 0.15$. Equation 1 is solved with boundary conditions that require $\varphi = 0.1$ V at the top of the system, and $\varphi = 0$ V at the bottom of the system to mimic the application of a 0.1 V potential difference in our experimental measurements. The 2D distribution of electrostatic potential is shown in figure 2, with the position of the nanochannel artificially darkened. Little variation in the potential is observed far from the nanochannel, and a strong decrease in electrostatic potential is observed within the channel. Qualitatively, our results resemble those obtained by others using similar PNP theories.[17,19]

In the second stage of the PNP calculation, the electrostatic potential is used to solve the Nernst-Planck equation to determine the charge carrier fluxes through the nanochannel:

$$\nabla \cdot \left[D_i \nabla c_i(\mathbf{r}) + \frac{D_i Z_i}{k_B T} c_i(\mathbf{r}) \nabla\varphi(\mathbf{r}) \right] = 0 \tag{2}$$
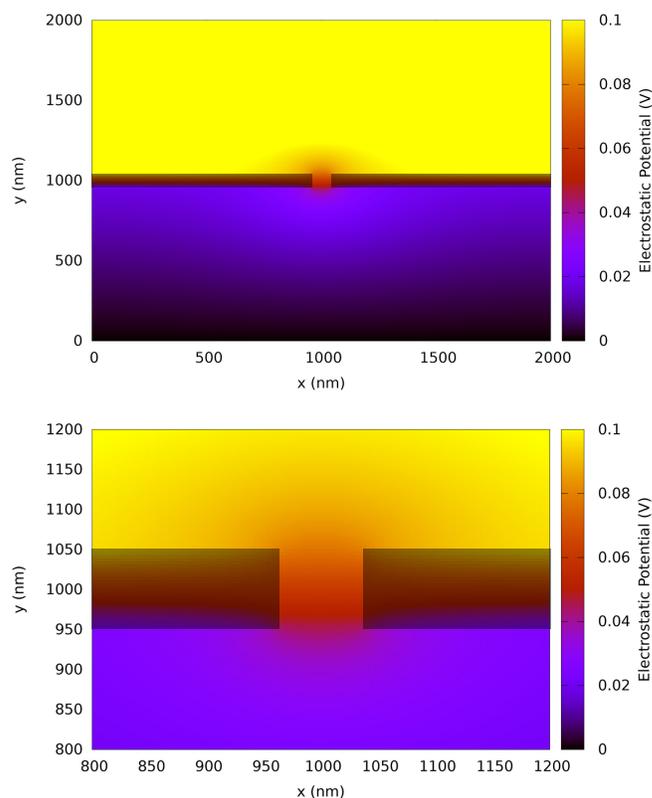
Fig. 2 Electrostatic potential for a nanochannel with diameter $d_P = 80$ nm and length $l_P = 100$ nm, with an applied voltage of $V = 0.1$ V. The position of the Si_3N_4 membrane is indicated by the artificially darkened regions.

where D_i and c_i are the diffusion coefficients and concentrations, respectively, of ion i, and Z_i is the charge carried by the ion (*e.g.*, $Z = e = 1.60 \times 10^{-19}$ C for K^+). We use $D_+ = 1.96 \times 10^{-5}$ cm^2/s for the potassium ion, and $D_- = 2.03 \times 10^{-5}$ cm^2/s for the chloride ion, and fix the equilibrium concentrations of both ions to be $c_0 = 1$ mol/L. Equations 1 and 2 are then solved self-consistently until the error in φ and c_i is below 10^{-7} and 10^{-6}, respectively. To aid in obtaining a numerical solution using the successive over-relaxation approach (SOR), equation 2 is converted to an equivalent form using a Slotboom transformation.[20] For simplicity, we assume that the K^+ and Cl^- ions have the same mobilities within the nanoparticles as they do in the bulk of the solution, and allow them to penetrate the interior of the nanoparticle at a concentration that is proportional to $(1 - h_{NP})$.

Upon completion of the PNP algorithm, the ion fluxes are calculated throughout the system according to:

$$j_i(\mathbf{r}) = -D_i \left[\nabla c_i(\mathbf{r}) + \frac{c_i Z_i}{k_B T} \nabla \varphi(\mathbf{r}) \right] \qquad (3)$$

The total ionic current through the channel is calculated from the integration of the ion flux across the channel:

$$i = F \int [j_+(\mathbf{r}) + j_-(\mathbf{r})] \, dA = F \int_0^{2\pi} \int_0^{d_P/2} [j_+(r) + j_-(r)] \, r \, dr \, d\theta \qquad (4)$$

where $F = eN_A$ is Faraday's constant, and N_A is Avogadro's number. The individual anion and cation currents can be calculated from their respective fluxes in the same fashion. Because of the axial symmetry in the system, our calculations are performed in two-dimensions and appropriately scaled to three-dimensions. An experimental i-V curve, and the PNP prediction, is shown in the Supporting Information, Figure S1. Interestingly, although the PNP result is close to the experimentally determined values, it slightly overpredicts the conductance of the channel. A similar behavior was also observed in Ref. 19. Because our Ag/AgCl electrodes detect the presence of chloride ions, we use the anion current from the PNP calculations to analyze our experimental translocation events.

4 Results and Discussion

Because standard SiO_2 nanoparticles are well-characterized, and can be treated as solid, spherical particles, we used them to validate the predictions of PNP calculations. Shown in Figure 3a is a typical translocation event for Ludox AM-30 SiO_2 nanoparticles, which are reported to have an average diameter of $d_{NP} \approx 7$ nm from the manufacturer. Recent work by Teulon *et al.*[21] reproduced this value from independent DLS measurements, but also found that the average diameter of these particles determined with other techniques such as transmission electron microscopy (TEM) or small-angle X-ray scattering (SAXS) deviated from this value. To illustrate this effect, we performed DLS measurements on the Ludox AM-30 nanoparticles and found the hydrodynamic radius $R_h \approx 14$ nm at $T = 298$ K with a diffusion coefficient of $D = 1.76 \times 10^{-7}$ cm^2/s. R_h is two times as large the size reported by the manufacturer. Translocation measurements find a value that is in much better agreement with the reported value of 7 nm.
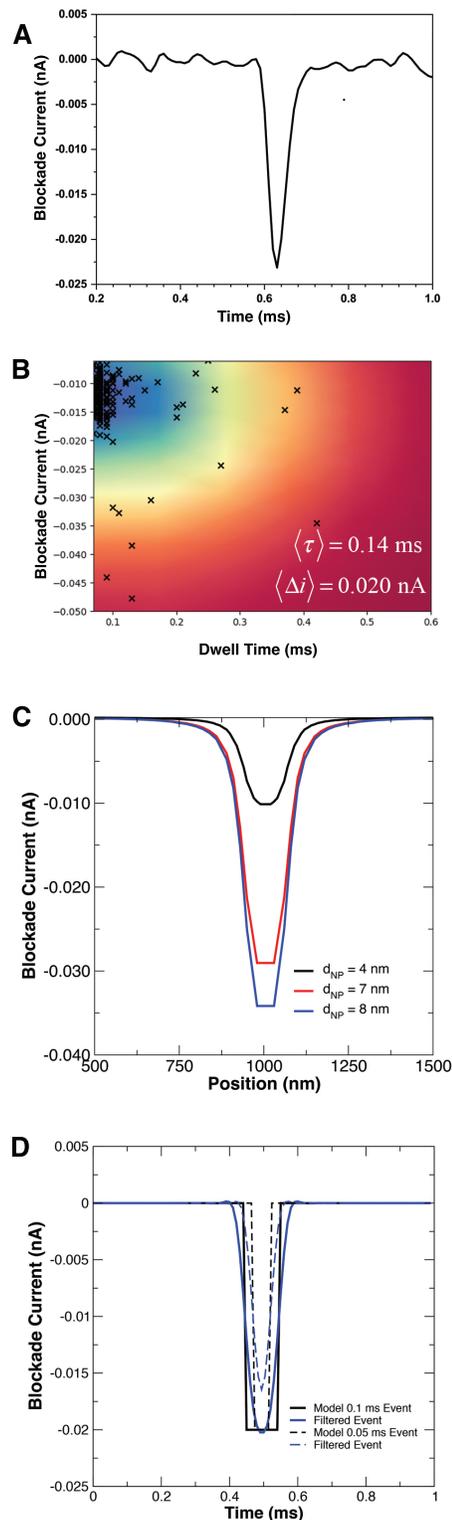
Fig. 3 Translocation characteristics of 7 nm Ludox SiO_2 nanoparticles. (a) Representative blockade event taken experimentally, showing a $\Delta i \approx 0.020$ nA current blockade across approximately $\tau \approx 0.1$ ms. (b) Histogram of blockade events, showing the highest density of events ($n = 211$) occurs for $\Delta i \sim 0.20$ nA, shown along with the average dwell time and blockade current. In the heat map, the blue region contains the highest density of translocation events, while red contains the lowest. (c) PNP calculations of a blockade event for a $d_{NP} = 4$, 7, and 8 nm particle with a hardness parameter $_{NP} = 1.00$ (top to bottom). The amplitude of the event for $d_{NP} = 7$ nm is $\Delta i = 0.030$ nA. (d) Simulated effect of a 10 kHz, 4-pole lowpass Bessel filter on the dwell time and blockade current of a 0.1 ms event (solid lines) and a 0.05 ms event (dashed lines).

For the translocation measurements in Figure 3, the nanochannel dimensions are $d_P = 80$ nm and $l_P = 100$ nm. The magnitude of the blockade current from this event ($\tau \approx 0.1$ ms) is approximately $\Delta i = 0.022$ nA. A 2D histogram of blockade current versus dwell time is shown in Figure 3b, from which we observe a high density of events in the vicinity of $\tau = 0.1$ ms and $\Delta i \approx 0.015$ nA. The average dwell time $\langle \tau \rangle$ and blockade current $\langle \Delta i \rangle$ for the SiO_2 nanoparticles are 0.14 ms and 0.020 nA, respectively. A PNP calculation of the translocation of three nanoparticles with varying diameters ($d_{NP} = 4$, 7, and 8 nm) through an 80 nm wide nanochannel is shown in Figure 3c. The calculations reproduce the expected signature of a blockade event, and the $d_{NP} = 7$ nm calculation is in close agreement with the experimentally measured values ($\Delta i_{PNP} = 0.030$ nA). From these calculations, we conclude that the average particle size is between 4 and 7 nm. Thus, PNP can reliably predict the expected translocation signals of bare SiO_2 nanoparticles – implying translocation measurements may be yet another technique with which we may obtain reliable physical properties on a *per particle basis*. Because of the high salt concentration in the system ([KCl] = 1 M), charges on the nanoparticle surfaces are screened and the particles are expected to behave as hard particles. Using the diffusion coefficient measured from DLS, we can estimate the amount of time required for a SiO_2 nanoparticle to traverse the $l_P = 100$ nm nanochannel due to Brownian motion alone as $\tau = l_P^2/6D \approx 0.1$ ms, which is also in quantitative agreement with the results from Figures 3a and 3b.

An important consideration in interpreting our measurements is the effect that the application of a 10 kHz lowpass Bessel filter has on the characteristics of translocation events. Due to high frequency noise, we are unable to resolve translocation events without the use of a lowpass filter. A recent paper from Robinson *et al.* found that instrumental filters can alter both the dwell times, characterized by the full width at half maximum of the signal, and the value of the blockade current.[22] Although we predict that the dwell times due to Brownian motion are on the order of 0.1 ms, this is near the lower limit below which a lowpass Bessel filter may attenuate the measured current. Shown in figure 3d are two idealized translocation events having dwell times of 0.1 ms (solid black line) and 0.05 ms (dashed black line). The amplitude of the signal is $\Delta i = 0.020$ nA to mimic the translocation of SiO_2 nanoparticles. After application of a 4-pole, lowpass Bessel filter (blue curves) we find that the amplitude and dwell time of the 0.1 ms event are maintained. However, a *ca.* 15% attenuation of the blockade current is observed for the 0.05 ms event. The implication of these results is that for events that occur on timescales below 0.1 ms, the 10 kHz hardware filter on the Axopatch 200B amplifier may need to be replaced with a higher frequency filter if the magnitude of the blockade current is to be used for determining the physical characteristics of nanoparticles. For the timescales we study in this work, the filter does not significantly alter the measured dwell times, since they are extracted using the CUSUM algorithm[16] and not the FWHM of the signal.

To further rationalize the value of the blockade current observed for SiO_2 nanoparticles, we can estimate the relative amount that the current should decrease. If the channel has an ohmic response, the ionic current can be written $i_0 = G_0 V$.
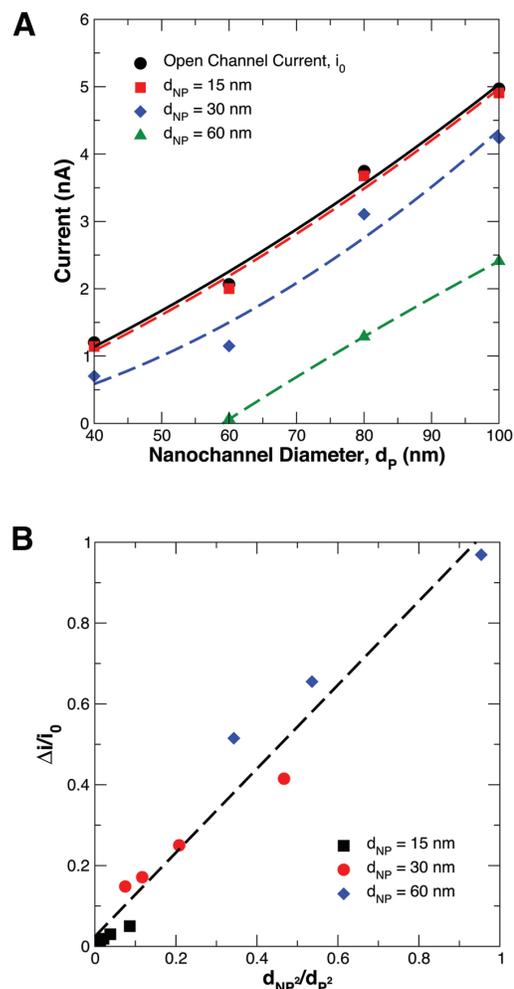
Fig. 4 (a) Dependence of current on nanochannel diameter from PNP calculations for three diameters of nanoparticle with a hardness factor of $h_{NP} = 1.00$ (*i.e.*, hard particles). The dashed lines are quadratic fits, reproducing the expected scaling of current with with d_P. (b) Relative decrease in current as a function of d_{NP}^2/d_P^2, taken from (a). The dashed line is a least-squares linear fit, with a slope of 1.03.

The open conductance of the nanochannel, when no particles are present, can be expressed as

$$G_0 = (\pi/4l_p)(\mu_{K^+} + \mu_{Cl^-})N_A c_0 e d_P^2 \quad (5)$$

where N_A is Avogadro's number, c_0 is the bulk ion concentration, e is the elementary charge, and $\mu_\pm$ is the mobility of the ion.[9] When a nanoparticle occludes the nanochannel, the conductance G decreases relative to G_0 and can be expressed as

$$G = (\pi/4l_p)(\mu_{K^+} + \mu_{Cl^-})N_A c_0 e(d_P^2 - d_{NP}^2) \quad (6)$$

which results in the characteristic pulse measured experimentally. Equations 5 and 6 imply that the relative size of the blockade event is

$$\frac{\Delta i}{i_0} = \frac{d_{NP}^2}{d_P^2} \quad (7)$$

For the $d = 7$ nm SiO$_2$ nanoparticles, $\Delta i/i_0 = 0.0076$. The open channel current from PNP calculations is $i_0 = 3.75$ nA, allowing us to estimate the blockade current as $\Delta i \approx 0.029$ nA. From the i-V curve (Supporting Information, Figure S1), we estimate $\Delta i = 0.019$ nA using the experimental open channel current. On the basis of these estimates, we conclude that the pulses observed experimentally are due to occlusion of the nanochannel by the particles.

Having validated our PNP calculations, we performed a series of calculations to determine the characteristics of blockade events for nanoparticles as a function of the nanoparticle diameter (d_{NP}) and channel diameter (d_P) in a 1 M KCl solution with a 0.1 V potential applied. Shown in Figure 4a is the chloride current as a function of nanochannel diameter for three sizes of hard nanoparticles (*i.e.*, $h_{NP} = 1.00$). The dashed lines are fits, showing the expected quadratic scaling of the current with d_P. As d_{NP} increases for a given value of d_P, the current decreases due to occlusion of the channel's cross-section. If equation 7 holds, then a plot of $\Delta i/i_0$ with respect to d_{NP}^2/d_P^2 should be linear. This plot is shown in Figure 4b along with a linear least-squares fit, which gives a slope of 1.03. Finally, as d_{NP}^2/d_P^2 decreases from 1 (complete blockage) to 0 (no blockage), the magnitude of the blockade current decreases from 100 % of the open channel current to 0 %, as expected. From these results, we conclude that PNP calculations give a valid estimation of the current and blockade current as both d_P and d_{NP} change, and recover the expected scaling relations for blockades resulting from physical occlusion of the nanochannel.

A histogram of blockade current versus dwell time for 154 phytoglycogen translocation events is shown in Figure 5 for a $d_P = 60$ nm channel. The phytoglycogen nanoparticles show a relatively tight grouping near $\tau = 0.1$ ms and $\Delta i = 0.005$ nA. Relative to the PNP calculations in Figure 4 for a $d_{NP} = 30$ nm diameter particle, the average blockade current for the phytoglycogen nanoparticle ($\langle \Delta i \rangle = 0.005$ nA) is several orders of magnitude smaller than the theoretical value ($\Delta i \approx 7.20$ nA). This is attributed to the fact that the nanoparticle is not hard, and water/ions can readily penetrate the interior of the nanoparticle. For this reason, the occlusion of the nanochannel is diminished. In the Supporting Information, we show that although PNP calculations find that the electrostatic potential does not vary significantly in response to
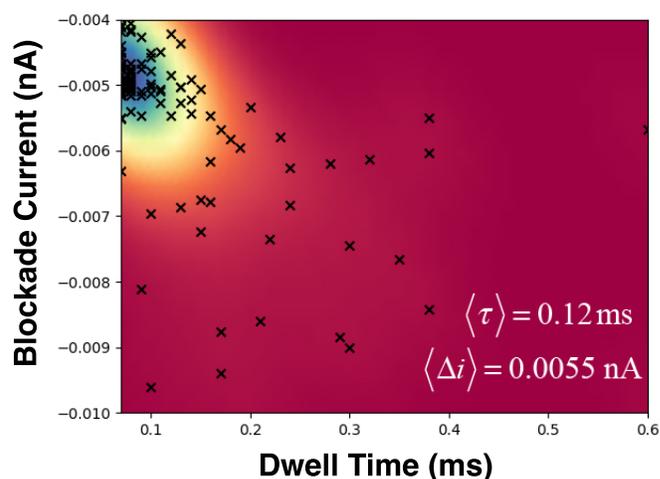
Fig. 5 Translocation characteristics of 35 nm phytoglycogen nanoparticles. The 2D histogram from $n = 154$ events shows an average dwell time of $\langle \tau \rangle = 0.12$ ms and an average blockade current of $\langle \Delta i \rangle = 0.0055$ nA. Blue regions correspond to a higher density of translocation events, while red regions correspond to a low density of translocation events.

changes in nanoparticle hardness (Figure S2), the concentration of ions within the nanochannel strongly depends on the nanoparticle hardness (h_{NP}, Figure S3). Thus, the reduction in the blockade current observed for the phytoglycogen nanoparticles is likely due to the fact that they are not solid particles and allow more ions to pass through the channel.

The histogram in Figure 5 also shows an asymmetric grouping of the translocation events, which slopes down and to the right (*i.e.*, to longer dwell times and larger blockade currents). This general shape is observed for all phytoglycogen translocation measurements we performed, and is discussed below. Interestingly, the average dwell time is very close to that measured for SiO$_2$ nanoparticles, which are more than 30% smaller than the phytoglycogen nanoparticles. DLS measurements of the phytoglycogen nanoparticles found a diffusion coefficient of $D = 7.9 \times 10^{-8}$ cm^2/s, on the basis of which we predict that the average dwell time for a phytoglycogen nanoparticle is $\tau = l_P^2/6D \approx 0.2$ ms.

2D histograms for 654 translocation events though a $d_P = 80$ nm nanochannel are shown in Figure 6a, with an average dwell time of $\langle \tau \rangle = 0.18$ ms and an average blockade current of $\langle \Delta i \rangle = 0.0058$ nA. In Figure 6b, analogous data are shown for 115 translocation events for a $d_P = 100$ nm nanochannel, which have an average dwell time of $\langle \tau \rangle = 0.20$ ms and an average blockade current of $\langle \Delta i \rangle = 0.0082$ nA. The average dwell times for both systems are similar, on the order of $\tau = 0.2$ ms, which is in excellent agreement with the value obtained by considering Brownian motion of the particle across the 100 nm length of the nanochannel. If the applied voltage is halved, the average dwell times remain constant while the blockade current decreases from $\langle \Delta i \rangle = 0.0082$ nA to 0.0064 nA ($d_P = 100$ nm, not shown), supporting the hypothesis that the nanoparticle motion is purely Brownian. For these reasons, we conclude that the data for the 80 nm and 100

A

B
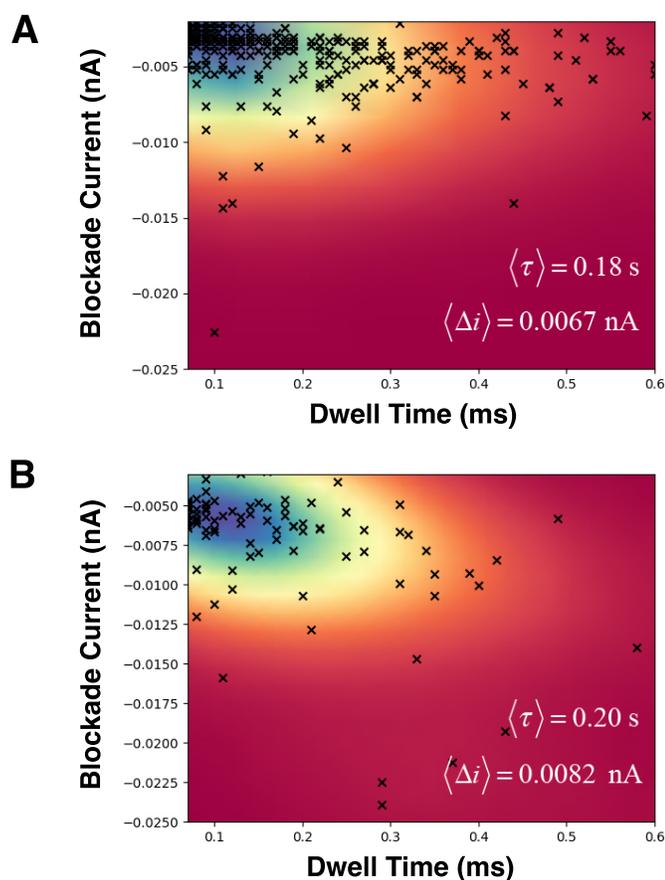
Fig. 6 Histograms of translocation characteristics for (a) $d_P = 80$ nm nanochannels ($n = 654$) and (b) $d_{NP} = 100$ nm nanochannels ($n = 115$). Blue regions correspond to a higher density of translocation events, while red regions correspond to a low density of translocation events.

Fig. 7 Blockade current as a function of h_{NP} for $d_{NP} = 30$ nm particles moving through $d_P = 60$ nm (squares), 80 nm (circles), and 100 nm (diamonds) diameter nanochannels. Lines are visual guides.

nm systems are representative of true translocation events. On the other hand, because the dwell time in the 60 nm system is much lower than for the larger diameter nanochannels, it is likely that the majority of the data in Figure 5 are not true translocation events, but "bounce-off" events where the particle enters the channel, but is not captured and returns its original fluid reservoir. This behavior can be further substantiated by considering the amplitude of the blockade events. To further substantiate the idea that the majority of events for the 60 nm nanochannels are "bounce-off" type events, we performed measurements with a $d_P = 40$ nm channel. The results, contained within the Supporting Information, have a similar shape to Figure 5, and an average dwell time of $\langle \tau \rangle \approx 0.15$ ms. The similar dwell times between the $d_P = 40$ nm and $d_P = 60$ nm imply that events in those two systems are more similar to each other than the $d_P = 80$ nm and $d_P = 100$ nm channels. Furthermore, the shape of the histograms is similar, with the vast majority of events tightly grouped near $\tau = 0.1$ ms. For all systems, the blockade currents are orders of magnitude lower than the PNP predictions for hard nanoparticles ($h_{NP} = 1.00$). Figure 6 displays an asymmetric shape of the histograms for both systems. The origin of the histogram asymmetry is discussed in more detail later.

Since it is known that the phytoglycogen nanoparticles are not hard particles, but rather highly branched saccharide chains, we performed PNP calculations as a function of the hardness parameter h_{NP} to predict the amplitude of the blockade events for nanoparticles with a fixed $d_{NP} = 30$ nm diameter. In Figure 7, we observe a decrease in the amplitude of the blockade current as the h_{NP} decreases. This behaviour is consistent with a less dense particle allowing more ions to flow through the interior of the particle. Also observed in Figure 7 is that for $h_{NP} < 0.25$, the magnitude of the blockade current decreases below $\Delta i \approx 0.030$ nA, which is more similar in magnitude to the values measured experimentally. In addition, as h_{NP} decreases, the blockade currents for the three nanochannel diameters converge at the smallest value of h_{NP} considered. However, even at the smallest value of h_{NP} in this series of calculations, the magnitude of Δi is still larger than the values measured experimentally.

To better connect the PNP calculations to the experimental measurements, we performed additional PNP calculations that systematically varied h_{NP} for nanoparticles with a fixed diameter of $d_{NP} = 35$ nm, and in $d_P = 60$, 80, and 100 nm nanochannels. The calculations indicated that to obtain blockades that matched experiments, $h_{NP} \approx 0.05$. The data are shown in Figure 8. Also in agreement with experiments, the variation of blockade current with the channel diameter is not strong. Within the error of our measurements, captured by the standard deviation in the experimental value of $\langle \Delta i \rangle$, we detect no appreciable difference in the blockade current, and cannot differentiate between the 80 nm and 100 nm diameter nanochannels experimentally. The value of h_{NP} that best describes the experimental data can be rationalized in terms of the neutron scattering measurements made by Nickels *et al.*[12] From SANS measurements, the authors of this work concluded that phytoglycogen nanoparticles are composed of $N_g = 2.59 \times 10^4$ glucose monomers, each of which has a volume of $v_g = 0.166$ nm^3, and $N_w = 5.85 \times 10^5$ water molecules, each with a volume $v_w = 0.030$ nm^3.[12] Because the blockage of ionic cur-
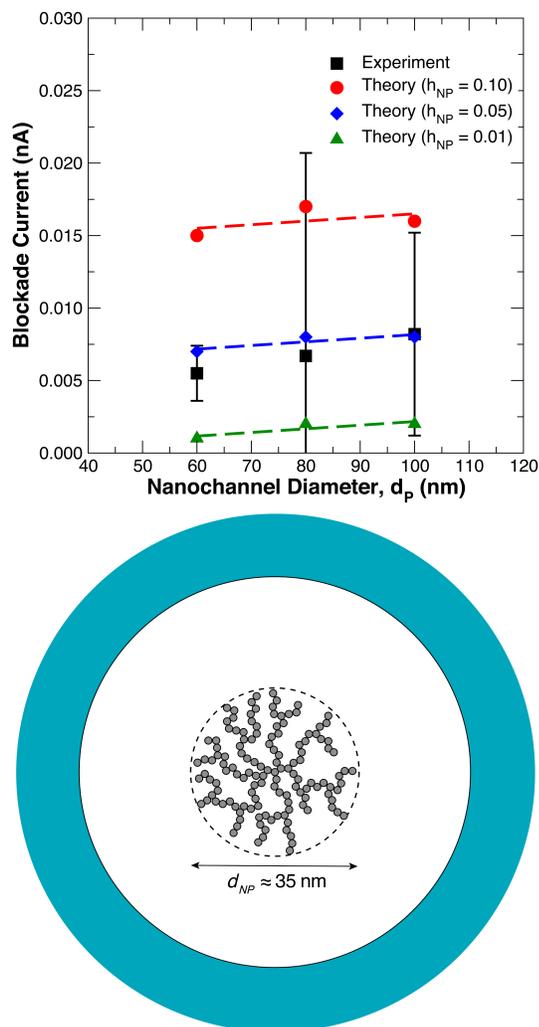
Fig. 8 Comparison between the magnitude of $\langle \Delta i \rangle$ from experiments (squares) and PNP calculations of a $d_{NP} = 35$ nm nanoparticle with $h_{NP} = 0.10$ (circles), $h_{NP} = 0.05$ (diamonds), and $h_{NP} = 0.01$ (triangles). Error bars correspond to one standard deviation in $\langle \Delta i \rangle$. The schematic below depicts the occlusion of a nanochannel by a phytoglycogen nanoparticle with diameter $d_{NP} = 35$ nm. Gray circles represent glucose monomers that fill the volume of the nanoparticle and block ion transport.

rent depends on the diameter of the nanoparticle,[9] h_{NP} should depend on the physical cross-sectional area of a phytoglycogen nanoparticle, as depicted in the schematic in Figure 8. Assuming the constituents are roughly spherical, then the diameter of each monomer and water molecule is approximately $d_g = 0.7$ nm and $d_w = 0.4$ nm, respectively. The hardness is given by $h_{NP} = N_g d_g^2/(N_g d_g^2 + N_w d_w^2)$. Assuming no overlap of monomers, we estimate $h_{NP} = 0.1$. If only 50% of the monomers contribute to the cross-sectional area of the nanoparticle (*e.g.*, the bottom hemisphere of the particle) then $N_g \rightarrow N_g/2$ and $h_{NP} = 0.06$. These rough estimates are in excellent agreement with the results from PNP calculations.

Because our translocation measurements provide us with the time required for a particle to move through the nanochannel (*i.e.*, dwell time), we can also extract a diffusion coefficient and a hydrodynamic radius for *each* nanoparticle that is detected. The

average diffusion coefficient and hydrodynamic radius from all events can be compared to DLS measurements to both check the accuracy of determining such quantities from translocation measurements, as well as to establish whether the nanoparticles are undergoing Brownian or electrophoretic motion. If the nanoparticles undergo Brownian motion during translocation, then for each particle, the diffusion coefficient can be expressed as:

$$D = \frac{l_P^2}{6\tau} \qquad (8)$$

where l_P is the length of the nanochannel, and τ is the particle's dwell time. For all of our measurements, $l_P = 100$ nm. Because "bounce-off" events do not represent true translocation events, we excluded them from the calculation of D by restricting our calculations to those for which $\tau > 0.1$ ms, and for which the diameter of the nanochannel $d_P > 60$ nm. From the recorded translocation events, we found $D = 8.76 \times 10^{-8}$ cm^2/s, which is close to the value measured using DLS (7.90×10^{-8} cm^2/s). Using the value of D obtained from translocation measurements, we find an average hydrodynamic radius of $R_h = 28$ nm, which is close to the DLS value of $R_h = 31$ nm. Thus, we have strong evidence that the translocation of the phytoglycogen nanoparticles is Brownian. Unfortunately, due to the size of the Ludox SiO$_2$ nanoparticles, the average translocation time is close to that of the "bounce-off" time for the phytoglycogen nanoparticles. Nevertheless, if we calculate the diffusion coefficient of the SiO$_2$ nanoparticles, excluding no events, we obtain $D = 1.88 \times 10^{-7}$ cm^2/s, which is close to the DLS value of $D = 1.76 \times 10^{-7}$ cm^2/s. From the calculated value of D, we obtain for the SiO$_2$ nanoparticles $R_h = 13$ nm, which is again close to the DLS value of 14 nm.

Figure 8 clarifies a few puzzling experimental observations. First, we observed that for $d_P = 60$ nm, the average dwell time $\langle \tau \rangle = 0.12$ ms, which was 50 % faster than expected for a 35 nm nanoparticle undergoing Brownian motion over a distance of 100 nm. In addition, for $d_P = 60$ nm, $\langle \Delta i \rangle = 0.005 \pm 0.002$ nA – which was the smallest *and* most precise value for our series of measurements. These two observations combined imply that the nanoparticles did not, on average, undergo translocation for the $d_P = 60$ nm system. The PNP calculations demonstrated that for $h_{NP} > 0.05$, the average blockade current should be larger than this value for real translocation processes, and the theoretical value falls outside of the error bars for the 60 nm system. Second, the 2D translocation histograms show a pronounced asymmetry in all systems measured, which corresponds to some translocation events blocking *more* current, and taking longer than expected for purely Brownian motion. A possible mechanism that gives rise to this asymmetry is shown in Figure 9. In Figure 9a, a single nanoparticle creates a blockade event (shown on the right) due to occlusion of the channel (denoted by the grey lines). The signature of this event is an blockade current of $\Delta i = 6$ pA which lasts $\tau = 0.2$ ms. In Figure 9b, two nanoparticles enter the nanochannel simultaneously, with positions that are offset from the center of the channel. This results in a slightly larger occlusion of the nanochannel, which in turn creates a larger blockade current, shown in the schematic to the right. The signature of these types of events in a 2D translocation histogram would be an asymmetry
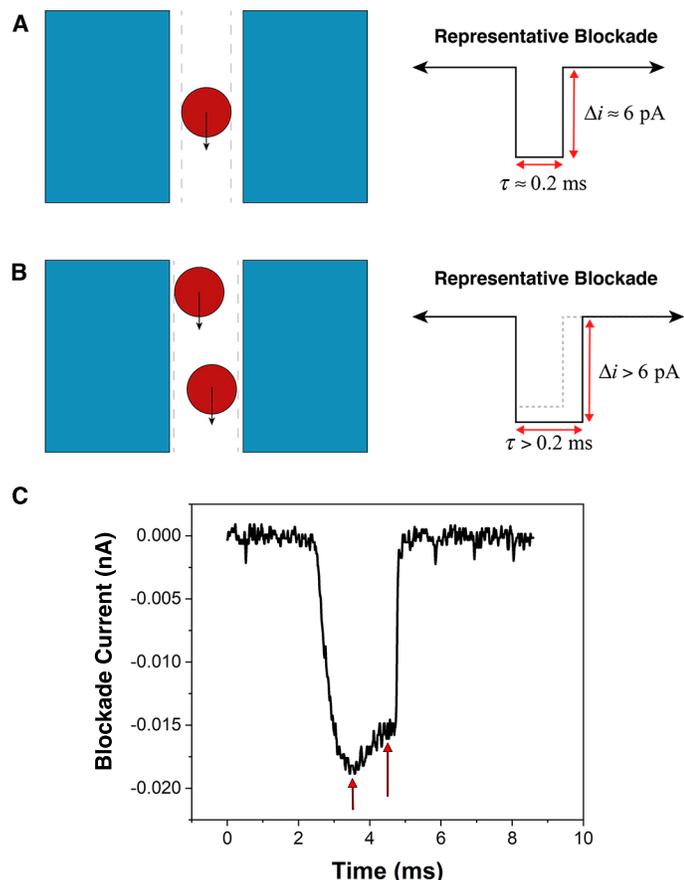
Fig. 9 Schematic of the translocation process. (a) A single nanoparticle moving through the nanochannel creates a blockade event, the depth of which is related to the diameter of the nanoparticle, relative to the nanochannel diameter, and the length of which is related to the diffusion coefficient of the nanoparticle. (b) Two nanoparticles simultaneously translocating, creating a larger occlusion of the nanochannel, illustrated by the dashed gray lines. Relative to (a) the blockade created is larger in amplitude and longer in time. (c) Blockade event for $d_P = 80$ nm of $\Delta i \approx 0.020$ nA and $\tau \approx 2$ ms. The two arrows show step increases in the blockade current over approximately 0.5 ms.

consistent with what we observe in our experiments. To support this hypothesis, in Figure 9c, a translocation event for a phytoglycogen nanoparticle through a $d_P = 80$ nm nanochannel shows a two-step increase in the blockade current, which occurs over $\tau \approx 0.5$ ms to 1 ms. The step increase in the current may be the signature of one particle exiting the nanochannel while another remains inside – leading to a small reduction in the magnitude of the blockade current. The time scale of the step increase is on the order of the time expected for a single nanoparticle to fully translocate. More experimental studies of this behaviour in the future, with additional theory and simulations, may lead to a greater understanding of these events, and give rise to the ability to determine additional nanoparticle characteristics on a per particle basis.

5 Conclusions

In summary, we have performed the first translocation measurements of soft phytoglycogen nanoparticles. Translocation was in-terpretted using Poisson-Nernst-Planck (PNP) calculations which were validated using standard SiO_2 nanoparticles. We modified our PNP calculations to account for a "hardness parameter" h_{NP} which describes the extent to which the solvent can pass through the interior of the nanoparticle. Experimentally, we measured average dwell times that are in quantitative agreement with values calculated when assuming Brownian motion of the particles with their diffusion coefficients ($\tau \approx 0.2$ ms). 2D histograms of the translocation data showed a slight asymmetry towards longer translocation times, and larger blockade currents. This asymmetry was ascribed to multiple particle events, and the possible signature of such events was observed experimentally. PNP calculations were found to be in excellent quantitative agreement with experiments, and allowed us to conclude that the phytoglycogen nanoparticles had hardness parameters $h_{NP} \approx 0.05$, which is in reasonable agreement with an estimate from previous studies by others.[12] In addition, analysis of the dwell times measured experimentally allowed us to extract diffusion coefficients and hydrodynamic radii that were in excellent agreement with values measured using dynamic light scattering (DLS).

Looking to the future, there are many opportunities to apply these techniques to other types of particles, including asymmetric particles, viruses, and complex polymer architectures. Nanochannel sensing is a powerful technique for obtaining physical characteristics on a per particle basis.[9] Measurements on other types of particle systems may in turn lead to increased understanding of viral infection, new types of nanoparticles that favour translocation, or in new water filtration strategies. Due to the challenging task of interpreting translocation signals, there are numerous opportunities to apply new theoretical techniques to advance the use of nanochannels in many sensing applications.

Conflicts of interest

There are no conflicts to declare.

Acknowledgements

Notes and references

1 V. V. Palyulin, T. Ala-Nissila and R. Metzler, *Soft Matter*, 2014, **10**, 9016–9037.

2 R. A. Jorgensen and W. J. Lucas, *Science Signaling*, 2006, **2006**, tr2–tr2.

3 Y. Benitez-Alfonso, C. Faulkner, C. Ritzenthaler and A. J. Maule, *Molecular Plant-Microbe Interactions*, 2010, **23**, 1403–1412.

4 T. Wei, A. Kikuchi, Y. Moriyasu, N. Suzuki, T. Shimizu, K. Hagiwara, H. Chen, M. Takahashi, T. Ichiki-Uehara and T. Omura, *Journal of Virology*, 2006, **80**, 8593–8602.

5 S. M. Bezrukov, I. Vodyanoy and V. A. Parsegian, *Nature*, 1994, **370**, 279–281.

6 I. M. Derrington, T. Z. Butler, M. D. Collins, E. Manrao, M. Pavlenok, M. Niederweis and J. H. Gundlach, *Proceedings of the National Academy of Sciences*, 2010, **107**, 16060–16065.

7 C. A. Merchant, K. Healy, M. Wanunu, V. Ray, N. Peterman, J. Bartel, M. D. Fischbein, K. Venta, Z. Luo, A. T. C. Johnson and M. Drndić, *Nano Letters*, 2010, **10**, 2915–2921.

8 K. Venta, G. Shemer, M. Puster, J. A. Rodríguez-Manzo, A. Balan, J. K. Rosenstein, K. Shepard and M. Drndić, *ACS Nano*, 2013, **7**, 4629–4636.

9 K. E. Venta, M. B. Zanjani, X. Ye, G. Danda, C. B. Murray, J. R. Lukes and M. Drndić, *Nano Letters*, 2014, **14**, 5358–5364.

10 G. Goyal, K. J. Freedman and M. J. Kim, *Analytical Chemistry*, 2013, **85**, 8180–8187.

11 G. Goyal, A. Darvish and M. J. Kim, *Analyst*, 2015, **140**, 4865–4873.

12 J. D. Nickels, J. Atkinson, E. Papp-Szabo, C. Stanley, S. O. Diallo, S. Perticaroli, B. Baylis, P. Mahon, G. Ehlers, J. Katsaras and J. R. Dutcher, *Biomacromolecules*, 2016, **17**, 735–743.

13 H. Shamana, M. Grossutti, E. Papp-Szabo, C. Miki and J. R. Dutcher, *Soft Matter*, 2018, **14**, 6496–6505.

14 M. Grossutti, E. Bergmann, B. Baylis and J. R. Dutcher, *Langmuir*, 2017, **33**, 2810–2816.

15 W.-J. Lan, M. A. Edwards, L. Luo, R. T. Perera, X. Wu, C. R. Martin and H. S. White, *Accounts of Chemical Research*, 2016, **49**, 2605–2613.

16 C. Raillon, P. Granjon, M. Graf, L. J. Steinbock and A. Radenovic, *Nanoscale*, 2012, **4**, 4916–4924.

17 M. Muthukumar and C. Y. Kong, *Proceedings of the National Academy of Sciences*, 2006, **103**, 5273–5278.

18 D. S. Bolintineanu, A. Sayyed-Ahmad, H. T. Davis and Y. N. Kaznessis, *PLOS Computational Biology*, 2009, **5**, 1–12.

19 L. van Oeffelen, W. Van Roy, H. Idrissi, D. Charlier, L. Lagae and G. Borghs, *PLOS ONE*, 2015, **10**, 1–16.

20 J. Slotboom and H. de Graaff, *Solid-State Electronics*, 1976, **19**, 857 – 862.

21 J.-M. Teulon, C. Godon, L. Chantalat, C. Moriscot, J. Cambedouzou, M. Odorico, J. Ravaux, R. Podor, A. Gerdil, A. Habert, N. Herlin-Boime, S.-w. W. Chen and J.-L. Pellequer, *Nanomaterials*, 2019, **9**, 2–29.

22 D. A. Robinson, M. A. Edwards, H. Ren and H. S. White, *ChemElectroChem*, **5**, 3059–3067.